ORIGINAL ARTICLE

Multi-Stimuli Responsive Luminescent β-Diketones and Difluoroboron Complexes with Heterocyclic Substituents

Fang Wang[1] · Daniel Song[1] · Diane A. Dickie[1] · Cassandra L. Fraser[1]

Abstract

Emissive β-diketones (bdks) and difluoroboron complexes (BF$_2$bdks) exhibit multi-stimuli responsive luminescence, including solvatochromism, viscochromism, aggregation induced emission, thermal and mechanochromic luminescence, halochromism and pH sensing. In this study, a series of six-membered heterocycle-substituted (piperidine, morpholine, 1-methyl piperazine) bdk ligands and boron complexes were synthesized, and their luminescent properties were investigated. All the compounds exhibited red-shifted emission in more polar solvents due to intramolecular charge transfer as well as higher emission intensity in more viscous environments. In response to solubility changes in water/tetrahydrofuran mixtures, while the piperazine bdk ligand showed aggregation caused quenching, the piperidine and morpholine bdks displayed enhanced emission upon aggregation. In the solid state, all ligands exhibited mechanochromism. More dramatic halochromism was observed for the piperidine boron dye spin cast film. In solution, for the boron dyes under varying pH values (1–13), different protonated and deprotonated forms were analyzed according to the measured emission spectra.

Keywords β-Diketone · Difluoroboron complex · Heterocycles · Multi-stimuli responsive luminescence · Six-membered ring

Introduction

Luminescent small molecules are important tools in biological probing and imaging applications [1]. By alteration of core scaffolds or substituent groups, customized luminescent dyes can be utilized as sensors in various environments [2]. Among those dyes, considerable interest is focused on compounds showing responsive emissions when subjected to external stimuli, such as changing polarity [3], viscosity [4], solubility [5] and pH [6], mechanical smearing and grinding [7], heating [8] and acid/base vapor annealing [9].

Solvatochromic dyes are sensitive to environmental polarity change and display changes in emission colors [10]. After light excitation, these compounds form a dipolar excited state

as a result of intramolecular charge transfer (ICT) between their electron donor and acceptor groups. Interaction of the excited dipole with varying solvent dipoles produces different emission colors [11]. Dyes with solvatochromism can be used to probe lipid order in model membranes and living cells [12, 13]. While solvatochromism illustrates change in emission wavelength, viscochromic dyes show different emission intensities in response to local viscosity changes [10]. These compounds contain freely rotating groups that twist in less viscous media, forming a twisted intramolecular charge transfer (TICT) state which promotes non-radiative decay of the excited molecules [11]. Viscous media prevent bond rotation and therefore increase fluorescence intensity. Similarly, dye aggregation due to poor solubility sterically causes restriction of intramolecular motions (RIM) such as restriction of intramolecular vibrations (RIV) and restriction of intramolecular rotations (RIR) [14, 15]. For luminescent compounds, this aggregation can result in aggregation caused quenching (ACQ) through non-radiative pathways via π-π bond interactions, unaffected emission, or aggregation induced emission (AIE), that is, enhanced emission when dye aggregates [16]. Dyes with AIE have been utilized as biosensors for carbohydrates, lipids, proteins, etc. [17]. For mechanochromic luminescent (ML) dyes in the solid state, external stimuli such as smearing and grinding can lead to dye emission color change

---

Fang Wang and Daniel Song are authors who contributed equally.

✉ Cassandra L. Fraser
  fraser@virginia.edu

[1] Department of Chemistry, University of Virginia, Charlottesville, VA 22904, USA

[18]. Other stimuli, thermally annealing (TA) and melt quenching (MQ), also result in emission wavelength changes due to alteration of the packing mode of the molecules [19, 20]. Typically, thermal annealing or heating leads to a more crystalline state, and melt quenching, smearing and grinding cause ML dyes to be more amorphous [21, 22]. Different emission colors can be observed in amorphous and crystalline states [23]. Dyes with ML properties have shown potential applications in light-emitting diodes and mechanical sensors [19]. Halochromic dyes are also capable of displaying altered emission color in response to acid or base vapor treatment in the solid state. A possible mechanism is that protonation or deprotonation of the compound through acid or base annealing respectively, affects the electron donating process in the molecule and thus results in emission wavelength changes [9]. In terms of changing pH values in solution, halochromic dyes show responsive emission color or intensity changes [6]. For example, a heteroatom-containing halochromic compound, 1-(4-pyridinyl)-1-phenyl-2-(9-carbazolyl) ethene, was reported to function as a fluorescent pH sensor in solution [24].

Difluoroboron β-diketones (BF₂bdks) are a series of luminescent dyes that show 1- and 2- photon absorption, color tunable emission as well as high quantum yields [25]. Additionally, previous reports demonstrate their multistimuli responsive luminescent properties both in solution and the solid state, indicating promise in sensing and imaging applications [22, 26, 27]. Previously, the effects of substituent ring size on the various stimuli-responsive properties were investigated, and the relationship between ring size and emission was determined [22]. In this study, a series of β-diketone (bdk) ligands and BF₂bdk dyes with six-membered nitrogen heterocycle substituents, piperidine, morpholine, 1-methyl piperazine, were synthesized and compared (Fig. 1). Multi-stimuli responsive luminescent properties were investigated, including solvatochromism, viscochromism, AIE, thermal and mechanochromism, halochromism and pH sensing. The purpose of this study is to explore the effects of different six-membered ring substituents on the various optical properties. It is hypothesized that the additional heteroatoms on the substituent ring would impact numerous luminescent properties such as solvatochromism (different electron-donating groups and ICT), mechanochromic luminescence (different intermolecular interactions and packing), and halochromism (different sensitivities to acid/base vapors and pH changes). The optical properties of the β-diketone ligands and BF₂bdk complexes in dichloromethane (DCM), including absorption and emission maxima, extinction coefficients, quantum yields and lifetimes, were also measured and compared.

Experimental Section

Materials

Solvents, tetrahydrofuran (THF) and CH_2Cl_2, were dried over 3 Å molecular sieves, which were activated at 300 °C before use, as previously reported [28]. All the chemicals used in this study were reagent grade and obtained from Alfa Aesar, TCI and Sigma-Aldrich. No further purification was needed. Silica TLC plates were used for monitoring reactions. The six-membered heterocycle substituted ketones used in the synthesis of the bdk ligands were prepared via a previously described method [29]. Data for L-pip and D-pip were obtained from ref. [22].

Methods

^{1}H NMR spectra were measured on a Varian NMRS 600 (600 MHz) instrument with $CDCl_3$ solvent. Peaks were referenced to the signal of residual protiochloroform at 7.26 ppm, and units of coupling constant were given in Hz. Mass spectrometry was performed utilizing a Micromass Q-TOF Ultima spectrometer, and electrospray ionization (ESI) method was adopted. Horiba Fluorolog-3 Model FL3-22 spectrofluorometer was used to take steady-state fluorescence spectra with double-grating excitation and emission monochromator. A Hewlett-Packard 8452A diode-array spectrophotometer was utilized for measuring UV–Vis spectra as well as extinction coefficients. A DataStation HUB SPC controller and a NanoLED-370 excitation source (λ_{ex} = 369 nm) were utilized to measure time-correlated single photon counting (TCSPC) fluorescence lifetimes, and data were analyzed by software DataStation v2.4 from Horiba Jobin Yvon. Fluorescence quantum yields of the morpholine and piperazine bdk ligands (L-mor and L-paz) in CH_2Cl_2 were measured using a dilute quinine sulfate in 0.1 M H_2SO_4 solution as a standard as previously described [30], with the values: ϕ_F (quinine sulfate in 0.1 M H_2SO_4) = 0.53 [30, 31], λ_{ex} = 366 nm, n_D^{20} (0.1 M H_2SO_4) = 1.333, n_D^{20} (CH_2Cl_2) = 1.424 [32]. Another standard, rhodamine 6G in EtOH, was utilized in the quantum
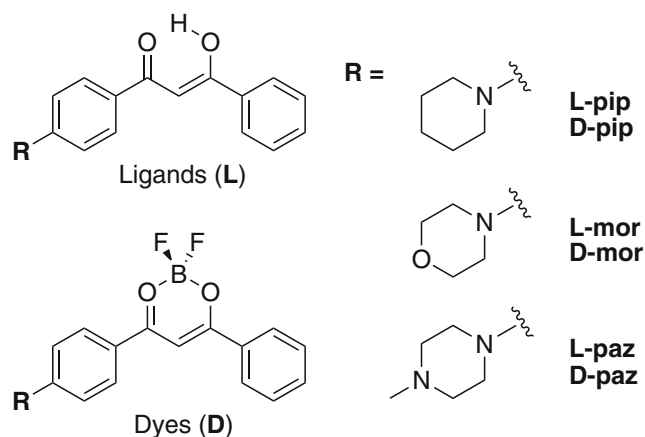

Fig. 1 Chemical structures of six-membered heterocycle substituted β-diketone ligands and difluoroboron complexes

R =

L-pip
D-pip

L-mor
D-mor

L-paz
D-paz

Ligands (L)

Dyes (D)

yield measurements of the morpholine and piperazine boron dyes in CH_2Cl_2 (D-mor and D-paz) [30], with the values: ϕ_F (rhodamine 6G in EtOH) = 0.94 [33], λ_{ex} = 488 nm, n_D^{20} (EtOH) = 1.361, n_D^{20} (CH_2Cl_2) = 1.424 [32]. A TA Instruments differential scanning calorimetry (DSC) 2920 Modulated DSC was used to take scans for the pristine powders of L-mor and L-paz. A 5 °C/min temperature ramp rate was set to record thermograms with the standard mode. For each sample, a second scan was collected and reported after the first conditioning cycle. The Universal Analysis Software V 2.3 from TA Instruments was utilized for DSC data analysis. A Mettler-Toledo GmbH 8603 pH meter was used to measure pH values of aqueous solutions.

Computational Details

The Gaussian 09 suite of programs was used to conduct density functional theory (DFT) calculations of the morpholine and piperazine substituted bdk ligands and boron complexes [34]. Ground state molecular geometry optimization was performed with B3LYP/6-31+G(d) and a Tomasi polarized continuum model in dichloromethane [35]. Vibrational frequency calculations were conducted using B3LYP/6-31+G(d), and all the obtained frequencies must be positive to continue the next step. Molecular orbital diagrams were then measured utilizing single point energy calculations with B3LYP/6-31G(d), and the calculated orbitals were visualized by software GaussView 5 [36]. Absorption spectra prediction for all the bdk ligands and difluoroboron complexes was conducted using time-dependent density functional theory (TD-DFT) with TDB3LYP/6-311+G(d).

Measurements in Solution

For optical properties, solvatochromism, viscochromism and AIE measurements, stock solutions of all the bdk ligands and boron dyes in CH_2Cl_2 were prepared. Calculated volumes of the stock solutions were transferred to empty vials, followed by evaporation of CH_2Cl_2 in air. A required volume of solvent or binary solvent mixture (dioxane/ethyl acetate (EtOAc), water/THF) was added to the vial to obtain 10^{-5} M solutions. Images under UV excitation, absorption and emission spectra were then measured. For pH sensing experiments, stock solutions of all the compounds were first prepared in dimethyl sulfoxide (DMSO), and appropriate volumes of the stock solutions were mixed with 10 mL of aqueous solution with different pH values (1–13), which were prepared using DI water, 1 M HCl and 1 M NaOH solutions.

Measurements in the Solid State

For studying thermal and ML properties of the morpholine and piperazine bdk ligands, ~10–20 mg compound powder was smeared on weighing paper, followed by thermally annealing (TA) at 110 °C in an oven for 10 min. The TA temperature was determined between the crystallization and melting points. A picture was taken under UV excitation and an emission spectrum was measured in the TA state. A heat gun was then used to heat and melt the sample for ~10 s, followed by cooling the weighing paper in air for 5 min. An image under UV light and an emission spectrum were taken in the melt quenched state. The spin cast films for halochromism experiments were prepared using 18×18 mm microscope coverslips. To fabricate the films, ~20 drops of saturated dye THF solution (~5 mg dye included) were dropped onto spinning coverslips (3000 rpm), followed by vacuum drying the spin cast films for 15 min.

Synthesis

Protons on the heterocycle substituted phenyl ring are labeled as primed.

(Z)-3-Hydroxy-1-(4-morpholinophenyl)-3-phenylprop-2-en-1-one (L-mor). The morpholine substituted ketone, 1-(4-morpholinophenyl)ethan-1-one (738 mg, 3.6 mmol), and methyl benzoate (450 μL, 3.6 mmol), were dissolved in anhydrous THF (20 mL). Sodium hydride in oil dispersion (60%, 432 mg, 10.8 mmol) in anhydrous THF (10 mL) was then added into the mixture via cannula transfer. The reaction was refluxed at 70 °C for 18 h under N_2 protection. When the morpholine substituted ketone was completely consumed, as monitored by TLC, the mixture was allowed to cool down to room temperature, followed by quenching with 1 M HCl (5 mL). Rotary evaporation was then conducted to remove THF. Extraction was performed afterwards with EtOAc (2 × 20 mL), and water (2 × 20 mL) and brine (2 × 20 mL) washes. For each wash or extraction, 1 M HCl (5 mL) was added to keep an acidic environment. The organic phase was then separated and dried with anhydrous Na_2SO_4, followed by filtration and rotary evaporation of the solvent. Recrystallization (CH_2Cl_2/hexanes) was conducted to purify the crude product to yield a yellow/green solid: 877.1 mg, 78.8%. ^1H NMR (600 MHz, $CDCl_3$): δ 17.06 (s, 1H, -O*H*), 7.96 (d, J = 6, 2H, 2, 6-Ar*H*), 7.93 (d, J = 6, 2H, 2′, 6′-Ar*H*), 7.52 (t, J = 6, 1H, 4-Ar*H*), 7.47 (t, J = 6, 2H, 3, 5-Ar*H*), 6.92 (d, J = 6, 2H, 3′, 5′-Ar*H*), 6.77 (s, 1H, COC*H*CO), 3.86 (t, J = 6, 4H, Ar-N(C*H$_2$*CH$_2$)$_2$O), 3.32 (t, J = 6, 4H, Ar-N(CH$_2$*CH$_2$*)$_2$O). HRMS (ESI, TOF) m/z calculated for $C_{19}H_{20}NO_3$, 310.1443 [M + H]$^+$; found 310.1448.

(Z)-3-Hydroxy-1-(4-(4-methylpiperazin-1-yl)phenyl)-3-phenylprop-2-en-1-one (L-paz). The piperazine substituted ligand was synthesized using the same method as L-mor. 1-(4-(4-methylpiperazin-1-yl)phenyl)ethan-1-one was used as the starting ketone replacing 1-(4-morpholinophenyl)ethan-1-one to yield a yellow solid: 488.0 mg, 67.8%. ^1H NMR (600 MHz, $CDCl_3$): δ 17.00 (s,

1H, -OH), 7.95 (d, $J = 6$, 2H, 2, 6-ArH), 7.93 (d, $J = 6$, 2H, 2′, 6′-ArH), 7.53 (t, $J = 6$, 1H, 4-ArH), 7.47 (t, $J = 6$, 2H, 3, 5-ArH), 6.93 (d, $J = 6$, 2H, 3′, 5′-ArH), 6.77 (s, 1H, COCHCO), 3.66 (s, 4H, Ar-N(CH$_2$CH$_2$)$_2$NCH$_3$), 3.01 (s, 4H, Ar-N(CH$_2$CH$_2$)$_2$NCH$_3$), 2.66 (s, 3H, Ar-N(CH$_2$CH$_2$)$_2$NCH$_3$). HRMS (ESI, TOF) m/z calculated for C$_{20}$H$_{23}$N$_2$O$_2$, 323.1760 [M + H]$^+$; found 323.1761.

(Z)-3-((Difluoroboraneyl)oxy)-1-(4-morpholinophenyl)-3-phenylprop-2-en-1-one (D-mor). The morpholine substituted boron complex was prepared by dissolving L-mor (214 mg, 0.69 mmol) in anhydrous CH$_2$Cl$_2$ (20 mL), followed by adding boron trifluoride diethyl etherate (111 µL, 0.90 mmol) via syringe. The reaction mixture was stirred at room temperature for 19 h under N$_2$ protection. When the reagent ligand was completely consumed, as determined by TLC, cold methanol (−20 °C, 80 mL) was added into the mixture to precipitate the product solid. After stirring 15 min, the mixture was filtered, and recrystallization (acetone/hexanes) was performed to purify the crude product to yield a red/orange solid: 78.4 mg, 31.8%. ^{1}H NMR (600 MHz, CDCl$_3$): δ 8.08 (t, $J = 6$, 4H, 2, 6-ArH, 2′, 6′-ArH), 7.62 (t, $J = 6$, 1H, 4-ArH), 7.51 (t, $J = 6$, 2H, 3, 5-ArH), 7.01 (s, 1H, COCHCO), 6.89 (d, $J = 12$, 2H, 3′, 5′-ArH), 3.86 (t, $J = 6$, 4H, Ar-N(CH$_2$CH$_2$)$_2$O), 3.44 (t, $J = 6$, 4H, Ar-N(CH$_2$CH$_2$)$_2$O). HRMS (ESI, TOF) m/z calculated for C$_{19}$H$_{19}$BF$_2$NO$_3$, 358.1426 [M + H]$^+$; found 358.1431.

(Z)-3-((Difluoroboraneyl)oxy)-1-(4-(4-methylpiperazin-1-yl)phenyl)-3-phenylprop-2-en-1-one (D-paz). The piperazine substituted boron complex was prepared using the same method as D-mor, but L-paz was used in place of L-mor to yield an orange solid: 18.2 mg, 14.9%. ^{1}H NMR (600 MHz, CDCl$_3$): δ 8.08 (t, $J = 12$, 4H, 2, 6-ArH, 2′, 6′-ArH), 7.62 (t, $J = 6$, 1H, 4-ArH), 7.52 (t, $J = 6$, 2H, 3, 5-ArH), 7.02 (s, 1H, COCHCO), 6.91 (d, $J = 6$, 2H, 3′, 5′-ArH), 3.67 (s, 4H, Ar-N(CH$_2$CH$_2$)$_2$NCH$_3$), 2.79 (s, 4H, Ar-N(CH$_2$CH$_2$)$_2$NCH$_3$), 2.54 (s, 3H, Ar-N(CH$_2$CH$_2$)$_2$NCH$_3$). HRMS (ESI, TOF) m/z calculated for C$_{20}$H$_{22}$BF$_2$N$_2$O$_2$, 371.1742 [M + H]$^+$; found 371.1746.

Results and Discussion

Synthesis and Optical Properties

The heterocycle substituted β-diketone ligands (**L**) were prepared via Claisen condensation [37]. The corresponding difluoroboron dyes (**D**) were synthesized by reaction of the bdk ligands with boron trifluoride diethyl etherate [38]. A series of optical properties for all the compounds were measured in 10^{-5} M CH$_2$Cl$_2$ solutions such as UV-vis absorption (λ_{abs}) and emission maxima (λ_{em}), quantum yields (ϕ), fluorescence lifetimes (τ) and extinction coefficients (ε) (Table 1).

Table 1 Optical properties of the six-membered ring substituted β-diketone ligands and boron complexes in CH$_2$Cl$_2$

Compound	λ_{abs}[a] (nm)	ε[b] (M^{-1} cm^{-1})	λ_{em}[c] (nm)	Φ[d]	τ[e] (ns)
L-pip	400	35,600	497	0.18	1.11
L-mor	384	30,700	479	0.51	1.51
L-paz	381	19,000	470	0.09	0.30
D-pip	466	60,400	542	0.02	1.81
D-mor	449	78,400	532	0.19	1.62
D-paz	448	39,000	504	0.03	2.60

[a] Absorbance maxima in air

[b] Extinction coefficient

[c] Fluorescence maxima in air ($\lambda_{ex} = 369$ nm)

[d] Quantum yield

[e] Fluorescence lifetime in air ($\lambda_{ex} = 369$ nm LED)

Data for L-pip and D-pip were obtained from ref. [22]

According to Table 1, all the BF$_2$bdk complexes show red-shifted absorption and emission maxima, higher extinction coefficients and lifetimes, but lower quantum yields than the corresponding bdk ligands. Those trends are commonly seen in amine ring substituted bdk ligands and BF$_2$bdk dyes [22, 26]. Comparing different rings, for both bdk ligands and boron dyes, the 1-methyl piperazine substituted compound displays the bluest absorption and emission, and the piperidine compound, the most red-shifted, due to different frontier molecular orbitals (FMOs) and intramolecular charge transfer processes with the additional heteroatoms. The highest quantum yields are observed for the morpholine substituted ligand and dye, and the lowest extinction coefficients can be found in the piperazine compounds. The fluorescence lifetime data were fit to double exponential decay, indicating multiple emissive species and absorption peaks, which are observed in the absorption and emission spectra of all the six-membered ring substituted compounds (Fig. S2). More details are discussed in the following computational section.

Computational Study

Density functional theory (DFT) calculations were conducted for geometry optimization and molecular orbital energies (Fig. 2 and Table S1). For all the shown compounds in Fig. 2, the electron density is distributed throughout the molecule in the lowest unoccupied molecular orbital (LUMO), and localized on the heterocycle substituted phenyl ring in the highest occupied molecular orbital (HOMO), which is similar to the charge distribution of the piperidine compounds in our previous study [22]. For HOMO-1, the morpholine substituted bdk ligand and boron dye have the most electron density on the unsubstituted phenyl ring side, however, the piperazine compounds show that the charge is localized on the

Fig. 2 Molecular orbitals of morpholine and 1-methyl piperazine substituted bdk ligands and BF$_2$bdk dyes
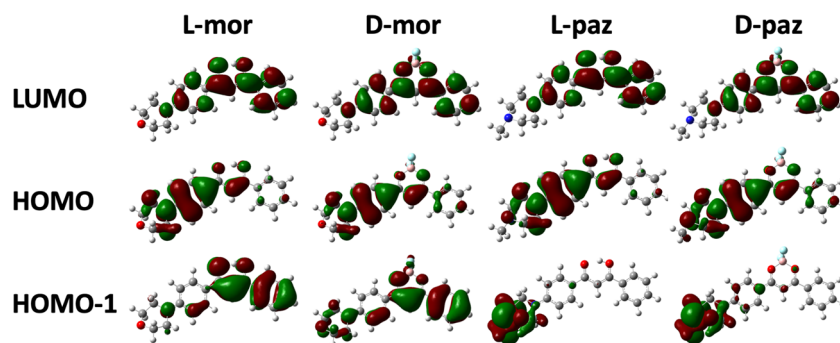
heterocycle. After analyzing the calculated excitation energies and oscillator strengths (f), it is shown that the dominating energy transition is from HOMO to LUMO (f_1: L-mor = 0.8655; D-mor = 1.1442; L-paz = 0.8581; D-paz = 0.9863), and the minor transition is from HOMO-1 to LUMO (f_2: L-mor = 0.3730; D-mor = 0.2590; L-paz = 0.0211; D-paz = 0.1862). Multiple energy transitions (e.g. HOMO to LUMO and HOMO-1 to LUMO) result in different absorption peaks and indicate multiple emissive species (Fig. S2). Based on the electron density map of the HOMO and LUMO, the primary energy transition from HOMO to LUMO exhibits intramolecular charge transfer (ICT), suggesting solvatochromism for all the compounds.

Solvatochromism

Given the ICT character illustrated by the DFT calculations, solvatochromism was tested for all the compounds in a series of solvents with differing polarities ($E_T(30)$ values from 33.7 for toluene to 46 for acetonitrile) [39, 40]. UV-excited images, absorption and emission spectra were taken for 10^{-5} M solutions of the selected solvents. For example, as shown in Fig. 3 and Table 2, L-mor maintained similar absorption wavelengths in different solvents, indicating that the ground state energy is essentially unaffected by changing solvent polarity. In more polar solvents, L-mor exhibited red-shifted emission, and dark emissions were observed in highly polar solvents such as acetone, methanol and acetonitrile, similar to previous findings with L-pip solvatochromism [22]. For the heterocycle substituted bdk ligands, both L-mor and L-paz displayed the bluest emission in toluene and the reddest in methanol (Fig. 3 and S3, Table 2). For the boronated dyes, the most blue-

shifted emission of D-mor was shown in toluene and the bluest emission of D-paz was found in 1,4-dioxane, while both dyes exhibited the most red-shifted emission in acetonitrile (Fig. S4 and S5). In order to compare the solvatochromism effects of all the six-membered ring substituted compounds, Lippert–Mataga plots (Stokes shifts $\Delta\nu$ versus solvent orientational polarizability $\Delta f'$, given TICT state was formed) were produced (Fig. S6). All the bdk ligands display linear relationships with positive slopes, substantiating dramatic solvatochromism. However, compared to the ligands, the R^2 correlation coefficients of the D-mor and D-paz plots are less than 0.5, and no clear trend can be found in the D-pip plot, suggesting less dramatic solvatochromism for the boron dyes. The slopes in the plots of the bdk ligands (L-pip: 2.7463; L-mor: 3.5208; L-paz: 2.7978) indicate the most dramatic solvatochromism in L-mor and the least dramatic in L-pip, which is probably due to different electron donating abilities of the six-membered heterocycles and thus different ICT processes.

Viscochromism

For all the compounds, viscochromism experiments were conducted in 1,4-dioxane/EtOAc solvent mixtures with the percentage of EtOAc ranging from 0 to 100% and consistent 10^{-5} M concentration. This solvent pair was chosen because of their different viscosities (EtOAc: 0.45 cP at 20 °C; dioxane: 1.37 cP at 20 °C) [41] but similar polarities ($E_T(30)$ value of EtOAc: 38.1 kcal mol^{-1}; dioxane: 36 kcal mol^{-1}) [40]. Therefore, the effects of changing solvent viscosities (by changing solvent mixture compositions) on the bdk ligands and boron dyes were investigated with minimizing the

Table 2 Absorption and emission maxima of L-mor in different solvents

Maxima	Toluene	Dioxane	Chloroform	DCM	THF	EtOAc	Acetone	MeOH	Acetonitrile
λ_{abs}[a] (nm)	381	383	381	384	385	381	381	385	385
λ_{em}[b] (nm)	442	458	465	479	473	472	494	516	501

[a] Absorption maxima in air

[b] Fluorescence maxima in air (λ_{ex} = 369 nm)

Fig. 3 Solvatochromism of L-mor: **a** UV-excited image of emissions in solvents with different polarities, **b** absorption spectra and **c** emission spectra in the indicated solvents (λ_{ex} = 369 nm)
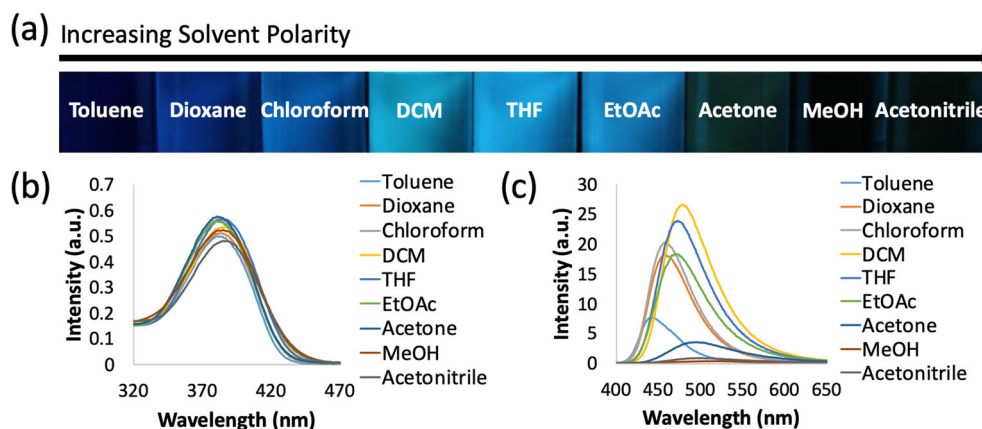
solvatochromism effects. According to Fig. S7, for all the compounds, the absorption spectra were similar in different solvent compositions, indicating that the ground state energy was not affected by environmental viscosity changes. Viscochromism properties of L-mor and L-paz are compared in Fig. 4. Upon increasing the fraction of EtOAc and thus decreasing the binary solvent viscosity, L-paz showed weakened emission but L-mor did not exhibit dramatic fluorescence intensity change. In addition, plots of relative emission intensity (I/I_0) against fraction of EtOAc (fe) for L-mor and L-paz are present in Fig. 4e and f, respectively. The piperazine bdk ligand displays a bigger absolute slope than the morpholine ligand (L-mor: 0.0016; L-paz: 0.0073), suggesting more dramatic viscochromism in L-paz. Comparing the boron dyes with the bdk ligands, D-mor showed more dramatic viscochromism than L-mor, however, in contrast, L-pip and L-paz exhibited higher viscosity sensitivity than their corresponding boron complexes (absolute slope numbers in the

plots of I/I_0 versus fe: 0.0016 for L-mor and 0.0061 for D-mor; 0.0057 for L-pip and 0.0016 for D-pip [22]; 0.0073 for L-paz and 0.0058 for D-paz) (Fig. 4 and S8).

Aggregation Induced Emission

The sensitivity of the bdk ligands and boron dyes to solubility changes was studied in a water/THF binary solvent system, where the compounds were well dissolved in THF but poorly soluble in water, inducing AIE. A series of solvent mixture compositions, ranging from 0 to 95% of water, were prepared, and the ligand or dye concentration was kept consistent as 10^{-5} M. UV-excited images, absorption and emission spectra were taken for all the compounds in different solvent compositions (Fig. 5, S9 and S10). The absorption spectra of all the bdk ligands and boron complexes showed dramatic absorbance increases at high water fractions (80%, 90% and 95%) owing to stronger light scattering, indicating aggregate

Fig. 4 Viscochromism: UV-excited images of **a** L-mor and **b** L-paz in dioxane/EtOAc mixtures with different fractions of EtOAc (fe), emission spectra of **c** L-mor and **d** L-paz (λ_{ex} = 369 nm), and plots of relative fluorescence intensity (I/I_0) versus fractions of EtOAc (fe) for **e** L-mor and **f** L-paz. Percentage error range: ±5%
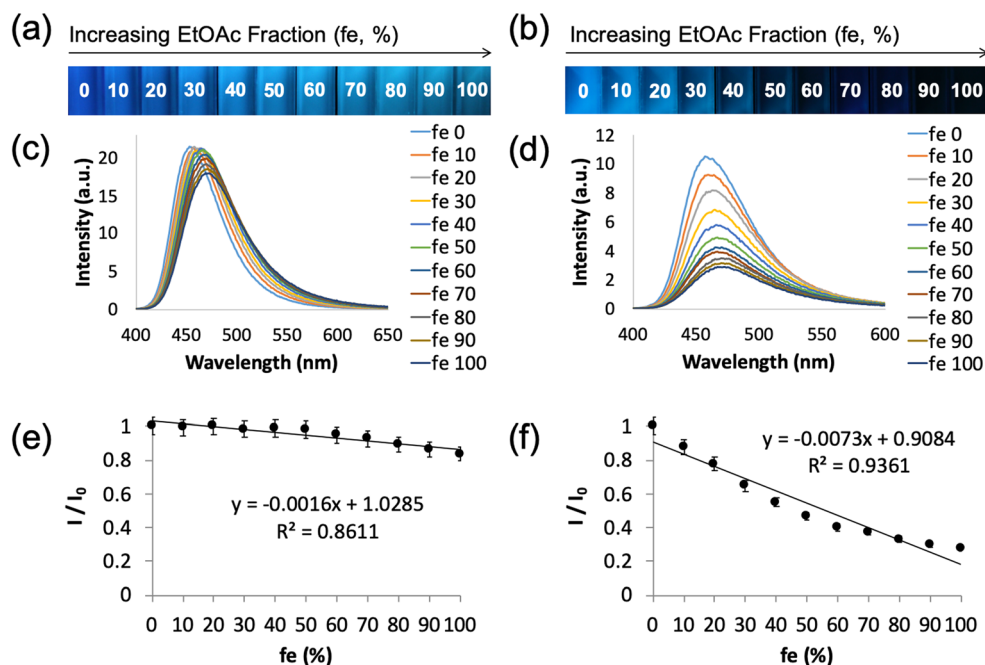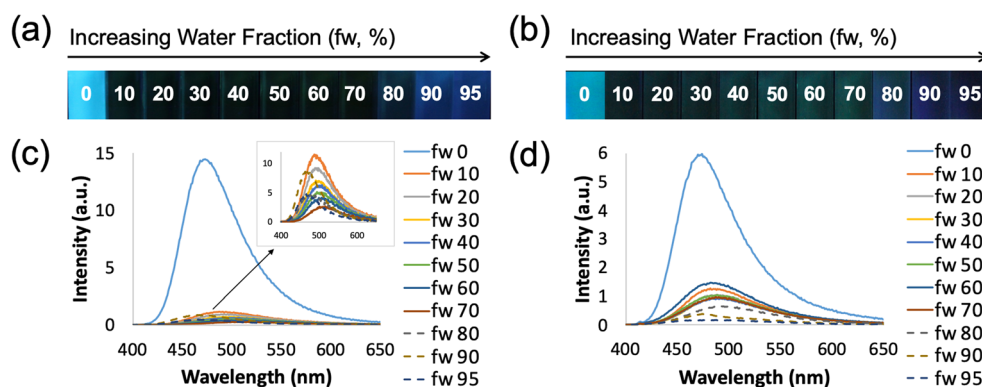
Fig. 5 UV-excited images of **a** L-mor and **b** L-paz in water/THF mixtures with different fractions of water (fw), and emission spectra of **c** L-mor and **d** L-paz (λ_{ex} = 369 nm). The spectra at water fractions of 80%, 90% and 95% are displayed in dashed lines

state formed in those solvent mixtures (Fig. S9). The AIE properties of L-mor and L-paz were analyzed and compared in Fig. 5. Both ligands exhibited bright emission in pure THF, followed by relatively dark emissions with increasing water fractions from 10 to 70%. For L-mor at water percentage of 80–95%, enhanced emissions with blue-shifted wavelengths (dashed spectra) were observed compared to 70% water (Fig. 5c), suggesting aggregation induced emission, which is similar to L-pip [22]. However, L-paz displayed quenched emission when aggregation happened at water fractions 80–95% (Fig. 5d, dashed spectra). For the boron complexes, both D-pip [22] and D-mor showed red-shifted emission with decreased intensity in the aggregate state. Aggregation caused quenching was also observed in D-paz without affecting the emission wavelength (Fig. S10).

Thermal and Mechanochromic Properties

Responsive luminescent properties of the bdk ligands and boron dyes to heating and molecular packing were investigated on weighing paper. Thermally annealed (TA) and melt quenched (MQ) states were studied and compared. Samples in the TA state were prepared by thermally annealing the compound-treated weighing paper at 110 °C, which was between the crystallization (T_c) and melting temperatures (T_m) determined by differential scanning calorimetry (DSC) (Fig. S11). Thus,

thermally annealing induced crystallization of the samples, and typically blue-shifts the emission [21, 23]. The MQ state was produced by melting and then cooling the sample weighing paper in air. Heating above the melting point led to the amorphous state, and typically red-shifted emission is observed compared to that in crystalline state [7, 42]. Preliminary screening did not show mechano-active properties for the boron complexes, so the bdk ligands were analyzed and compared for their thermal and ML properties. For all the bdk ligands, bathochromic emission was observed in the MQ state compared to the TA state (Fig. 6). Among these ligands, L-pip exhibited the greatest emission wavelength shift (L-pip: 45 nm [22], L-mor: 23 nm, L-paz: 20 nm). Single crystals of L-mor were grown from THF/n-pentane using a vapor diffusion method, and the packing details were analyzed and compared with those of L-pip [22] to better understand the relationship between packing structure and ML properties. A complete list of intermolecular interactions is included for L-pip (Table S2) and L-mor (Table S3). More intermolecular contacts are found in the L-mor crystal structure than L-pip, and L-mor displays shorter contact distances than L-pip (C–H···arene interactions: 2.738 Å for L-mor and 2.759 Å for L-pip; C–H···O hydrogen bonding: 2.603 Å for L-mor and 2.619 Å for L-pip) (Fig. 7a and b), indicating tighter packing and less flexibility in the L-mor structure and thus less dramatic mechanochromism than the piperidine ligand. Comparing the unit cells of the two
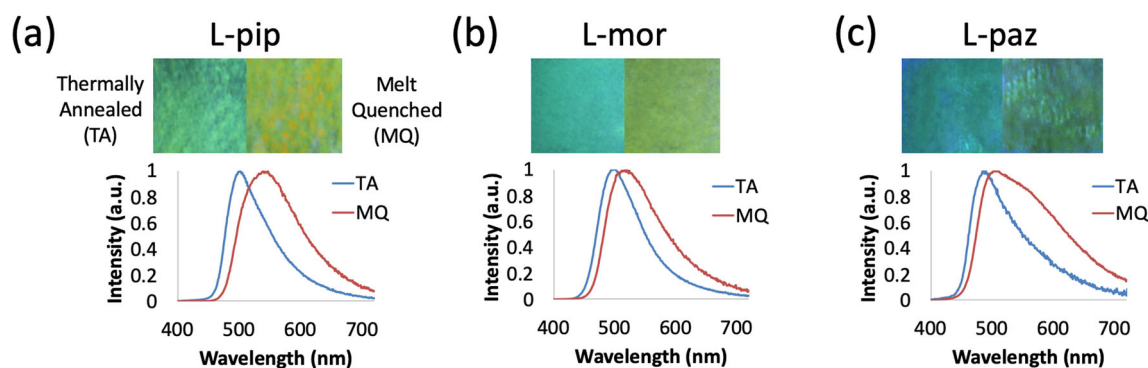

Fig. 6 Thermal and mechanochromic luminescence: UV-excited images and emission spectra of **a** L-pip, **b** L-mor and **c** L-paz in thermally annealed (TA) and melt quenched (MQ) states (λ_{ex} = 369 nm). Data for L-pip were obtained from ref. [22]

Fig. 7 Single crystal structure details: intermolecular interactions of **a** L-mor and **b** L-pip, and the unit cells of **c** L-mor and **d** L-pip. Data for L-pip were obtained from ref. [22]
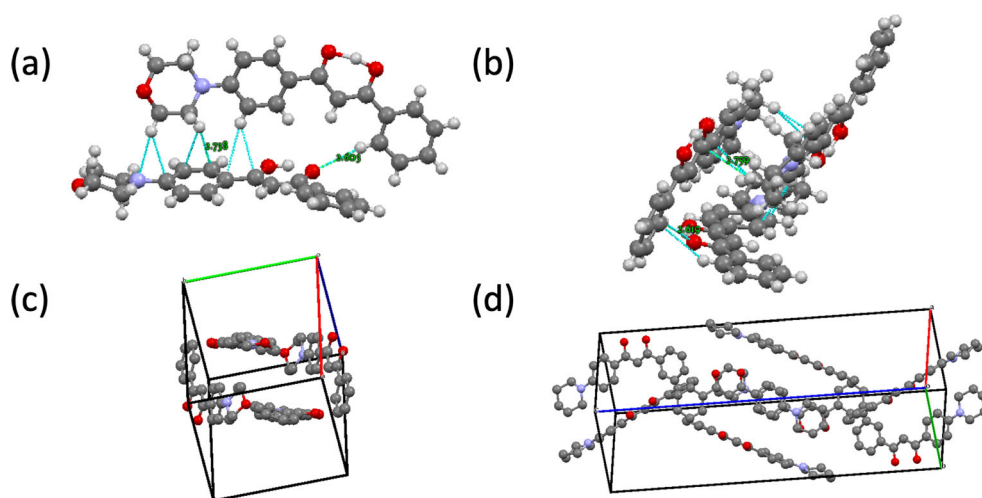
bdk ligands in Fig. 7c and d, offset dimer formation is observed only in L-pip, which is typically a predictor of good ML in β-diketone materials [20]. This accounts for more dramatic ML in L-pip than L-mor.

Halochromism and pH Sensing

Halochromism was investigated in both solution and the solid state. These experiments concentrated on the boron complexes for comparison with a previous study [22]. First, in the solid state, trifluoroacetic acid (TFA) and triethylamine (TEA) were used to vapor anneal the spin cast films. The piperidine boron dye showed blue-shifted emission after acid annealing (AA) the as spun (AS) films, and base annealing (BA) resulted in partial recovery of the emission to green [22]. However, for the morpholine and piperazine dyes, less dramatic halochromism was observed without shifting the emission wavelength as much as D-pip in the AA and BA states (Fig. 8). A possible explanation is that the lone pairs of the additional oxygen or nitrogen atom (i.e. not directly attached to the aryl ring) are more basic than the aniline nitrogen, and thus, are protonated first. This is reasonable given substituted anilines are highly sensitive to substituent effects. Protonation of N or O heteroatoms could hinder further protonation of the aniline nitrogen, leading to less molecular orbital change and emission wavelength shift.

In order to ensure sufficient interaction between the dye molecules and acid/base, halochromism and pH sensing properties of all the boron dyes were also explored in aqueous solutions with different pH values, ranging from 1 to 13. The dyes were dissolved in dimethyl sulfoxide and then mixed with water to achieve an overall concentration of 10^{-5} M, and emission spectra were obtained. According to Fig. 9a, at pH 1 and 2, protonation of piperidine caused the electron donor to function as an acceptor group instead, and consequently, changed FMO energy and blue-shifted the emission (~407 nm). The original D-pip molecules were present with red emissions at pH 2–10. For D-mor at pH 1, double protonation occurred at the nitrogen and oxygen sites in the morpholine ring, and hypsochromic emission was observed (~398 nm) (Fig. 9b). From pH 2–7, single protonated D-mor on the morpholine oxygen atom (referring to the minor emission peak) and the original molecules (referring to the primary emission peak) coexisted in the solutions and reached dynamic equilibria. Only the original form of the compound was evident in solutions at pH 8–10. Finally, for D-paz, as shown in Fig. 9c and d, both single and double protonated forms were present at pH 1–4 with emission wavelengths at ~542 nm and ~403 nm, respectively. As pH increased from 5 to 10, both forms were deprotonated to the original molecule and red emission was observed. All the boron dyes were hydrolyzed to the corresponding bdk ligands at high pH 10–13, and were deprotonated in the basic environments, which is supported by
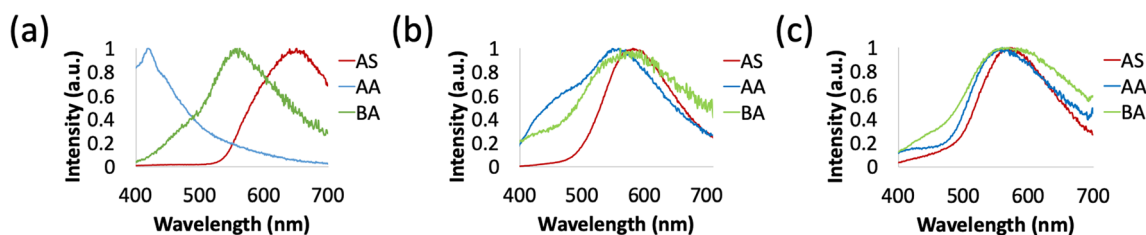

Fig. 8 Solid-state halochromism: normalized emission spectra of **a** D-pip, **b** D-mor and **c** D-paz in as spun (AS), acid annealed (AA) and base annealed (BA) states ($\lambda_{ex} = 369$ nm). Data for D-pip were obtained from ref. [22]
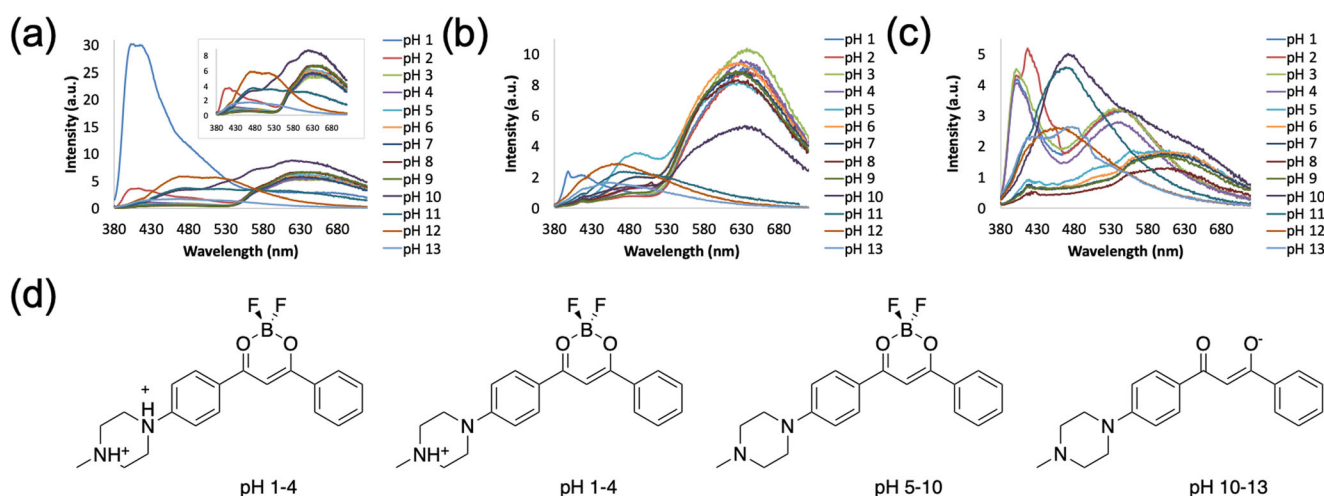
Fig. 9 Halochromism and pH sensing properties: emission spectra of **a** D-pip, **b** D-mor and **c** D-paz in aqueous solutions with pH values ranging from 1 to 13 ($\lambda_{ex} = 369$ nm), and **d** proposed molecular structures of the piperazine compound at varying pH values

their emission wavelengths matching those of the bdk ligands at corresponding pH values (Fig. S12).

Conclusion

In summary, a series of β-diketones and difluoroboron complexes were synthesized with six-membered heterocycle substituents in the 4-position (i.e. piperidine, morpholine and 1-methyl piperazine), and multiple stimuli-responsive luminescent properties were explored. In CH$_2$Cl$_2$, for both bdk ligands and boron dyes, the piperidine compound showed the most red-shifted absorption and emission and the piperazine compound the most blue-shifted. The morpholine substituted ligand or dye displayed the highest quantum yields than the other two substituents. Intramolecular charge transfer character was revealed by density functional theory calculations, indicating sensitivity to solvent polarity change for all the compounds. This was verified by solvatochromism experiments, where all the ligands and dyes exhibited bathochromic emissions in more polar solvents, indicating their potential use in probing polarity change and phase separation in biomembranes. Comparing different heterocycle substituted bdk ligands, L-mor exhibited the most dramatic solvatochromism and L-pip the least. In addition, all the compounds showed increased fluorescence intensity in more viscous solutions, suggesting promise in rigidity or viscosity sensing applications. In the aggregate state, L-paz and all the studied boron dyes displayed quenched emission, while red-shifted emission was observed for D-mor. Increased emission intensity and blue-shifted wavelength were found in L-pip and L-mor when they aggregated in high water fractions, which is AIE. Thermal and mechanochromic properties were investigated on weighing paper. All the bdk ligands exhibited red-shifted emission in the melt quenched state compared to the

thermally annealed state, and L-pip showed more dramatic emission wavelength shift than the other two ligands, due to loose molecular packing and offset dimer formation. Furthermore, halochromism tests on spin cast films suggest more sensitive emission for D-pip to acid/base vapor annealing. In aqueous solutions with different pH values (1–13), all the boron complexes showed sensitivity to pH change, and various forms of molecule (original, hydrolyzed, single and double protonated forms) with varying emissions were present in different pH ranges. This property can find application in sensing pH changes in biological systems.

Data Availability The authors declare that the data supporting the findings of this study are available in the article and the supplementary materials. Data for L-pip and D-pip were obtained from ref. [22].

Compliance with Ethical Standards

Conflict of Interest The authors declare no conflict of interest.

Code Availability Not applicable.

References

1. Lavis LD, Raines RT (2008) Bright ideas for chemical biology. ACS Chem Biol 3:142–155. https://doi.org/10.1021/cb700248m
2. Lavis LD, Raines RT (2014) Bright building blocks for chemical biology. ACS Chem Biol 9:855–866. https://doi.org/10.1021/cb500078u
3. Marini A, Munnoz-Losa A, Biancardi A, Mennucci B (2010) What is solvatochromism? J Phys Chem B 114:17128–17135. https://doi.org/10.1021/jp1097487
4. Kuimova MK, Yahioglu G, Levitt JA, Suhling K (2008) Molecular rotor measures viscosity of live cells via fluorescence lifetime

imaging. J Am Chem Soc 130:6672–6673. https://doi.org/10.1021/ja800570d

5. Luo J, Xie Z, Lam JWY, Cheng L, Chen H, Qiu C, Kwok HS, Zhan X, Liu Y, Zhu D, Tang BZ (2001) Aggregation-induced emission of 1-methyl-1,2,3,4,5-pentaphenylsilole. Chem Commun 381:1740–1741. https://doi.org/10.1039/b105159h

6. Zhang X, Rehm S, Safont-Sempere MM, Würthner F (2009) Vesicular perylene dye nanocapsules as supramolecular fluorescent pH sensor systems. Nat Chem 1:623–629. https://doi.org/10.1038/nchem.368

7. Zhang G, Lu J, Sabat M, Fraser CL (2010) Polymorphism and reversible mechanochromic luminescence for solid-state difluoroboron avobenzone. J Am Chem Soc 132:2160–2162. https://doi.org/10.1021/ja9097719

8. Park SK, Cho I, Gierschner J, Kim JH, Kim JH, Kwon JE, Kwon OK, Whang DR, Park JH, An BK, Park SY (2016) Stimuli-responsive reversible fluorescence switching in a crystalline donor-acceptor mixture film: mixed stack charge-transfer emission versus segregated stack monomer emission. Angew Chemie - Int Ed 55:203–207. https://doi.org/10.1002/anie.201508210

9. Yoshii R, Hirose A, Tanaka K, Chujo Y (2014) Functionalization of boron diiminates with unique optical properties: multicolor tuning of crystallization-induced emission and introduction into the main-chain of conjugated polymers. J Am Chem Soc 136:18131–18139. https://doi.org/10.1021/ja510985v

10. Klymchenko AS (2017) Solvatochromic and fluorogenic dyes as environment-sensitive probes: design and biological applications. Acc Chem Res 50:366–375. https://doi.org/10.1021/acs.accounts.6b00517

11. Grabowski ZR, Rotkiewicz K, Rettig W (2003) Structural changes accompanying intramolecular electron transfer: focuson twisted intramolecular charge-transfer states and structures. Chem Rev 103:3899–4032. https://doi.org/10.1021/cr940745l

12. Kucherak OA, Oncul S, Darwich Z, Yushchenko DA, Arntz Y, Didier P, Mély Y, Klymchenko AS (2010) Switchable nile red-based probe for cholesterol and lipid order at the outer leaflet of biomembranes. J Am Chem Soc 132:4907–4916. https://doi.org/10.1021/ja100351w

13. Klymchenko AS, Kreder R (2014) Fluorescent probes for lipid rafts: from model membranes to living cells. Chem Biol 21:97–113. https://doi.org/10.1016/j.chembiol.2013.11.009

14. Wang H, Zhao E, Lam JWY, Tang BZ (2015) AIE luminogens: emission brightened by aggregation. Mater Today 18:365–377. https://doi.org/10.1016/j.mattod.2015.03.004

15. Mei J, Leung NLC, Kwok RTK, Lam JWY, Tang BZ (2015) Aggregation-induced emission: together we shine, united we soar! Chem Rev 115:11718–11940. https://doi.org/10.1021/acs.chemrev.5b00263

16. Hong Y, Lam JWY, Tang BZ (2011) Aggregation-induced emission. Chem Soc Rev 40:5361–5388. https://doi.org/10.1039/c1cs15113d

17. Kwok RTK, Leung CWT, Lam JWY, Tang BZ (2015) Biosensing by luminogens with aggregation-induced emission characteristics. Chem Soc Rev 44:4228–4238. https://doi.org/10.1039/c4cs00325j

18. Butler T, Morris WA, Samonina-Kosicka J, Fraser CL (2016) Mechanochromic luminescence and aggregation induced emission of dinaphthoylmethane β-diketones and their boronated counterparts. ACS Appl Mater Interfaces 8:1242–1251. https://doi.org/10.1021/acsami.5b09688

19. Sagara Y, Kato T (2009) Mechanically induced luminescence changes in molecular assemblies. Nat Chem 1:605–610. https://doi.org/10.1038/nchem.411

20. Sun X, Zhang X, Li X, Liu S, Zhang G (2012) A mechanistic investigation of mechanochromic luminescent organoboron materials. J Mater Chem 22:17332–17339. https://doi.org/10.1039/c2jm32809g

21. Zhang G, Singer JP, Kooi SE, Evans RE, Thomas EL, Fraser CL (2011) Reversible solid-state mechanochromic fluorescence from a boron lipid dye. J Mater Chem 21:8295–8299. https://doi.org/10.1039/c0jm03871g

22. Wang F, Song D, Dickie DA, Fraser CL (2019) Ring size effects on multi-stimuli responsive luminescent properties of cyclic amine substituted β-diketones and difluoroboron complexes. Chem - An Asian J 14:1849–1859. https://doi.org/10.1002/asia.201801576

23. Ito H, Saito T, Oshima N, Kitamura N, Ishizaka S, Hinatsu Y, Wakeshima M, Kato M, Tsuge K, Sawamura M (2008) Reversible mechanochromic luminescence of [(C$_6$F$_5$Au)$_2$(μ-1,4-diisocyanobenzene)]. J Am Chem Soc 130:10044–10045. https://doi.org/10.1021/ja8019356

24. Yang Z, Qin W, Lam JWY, Chen S, Sung HHY, Williams ID, Tang BZ (2013) Fluorescent pH sensor constructed from a heteroatom-containing luminogen with tunable AIE and ICT characteristics. Chem Sci 4:3725–3730. https://doi.org/10.1039/c3sc50648g

25. Tanaka K, Chujo Y (2015) Recent progress of optical functional nanomaterials based on organoboron complexes with β-diketonate, ketoiminate and diiminate. NPG Asia Mater 7:223–315. https://doi.org/10.1038/am.2015.118

26. Wang F, DeRosa CA, Daly ML, Song D, Sabat M, Fraser CL (2017) Multi-stimuli responsive luminescent azepane-substituted β-diketones and difluoroboron complexes. Mater Chem Front 1:1866–1874. https://doi.org/10.1039/C7QM00137A

27. Wang F, DeRosa CA, Song D, Dickie DA, Fraser CL (2019) Environment-sensitive azepane-substituted β-diketones and difluoroboron complexes with restricted C–C bond rotation. J Phys Chem C 123:23124–23130. https://doi.org/10.1021/acs.jpcc.9b06304

28. Williams DBG, Lawton M (2010) Drying of organic solvents: quantitative evaluation of the efficiency of several desiccants. J Org Chem 75:8351–8354. https://doi.org/10.1021/jo101589h

29. Watson AJA, Fairbanks AJ (2013) Ruthenium-catalyzed transfer hydrogenation of amino- and amido-substituted acetophenones. Eur J Org Chem 2013:6784–6788. https://doi.org/10.1002/ejoc.201301020

30. Heller CA, Henry RA, McLaughlin BA, Bliss DE (1974) Fluorescence spectra and quantum yields. Quinine, uranine, 9,10-diphenylanthracene, and 9,10-bis(phenylethynyl)anthracenes. J Chem Eng Data 19:214–219. https://doi.org/10.1021/je60062a002

31. Melhuish WH (1961) Quantum efficiencies of fluorescence of organic substances: effect of solvent and concentration of the fluorescent solute. J Phys Chem 65:229–235. https://doi.org/10.1021/j100820a009

32. Saunders JE, Sanders C, Chen H, Loock H-P (2016) Refractive indices of common solvents and solutions at 1550 nm. Appl Opt 55:947–953. https://doi.org/10.1364/AO.55.000947

33. Kubin RF, Fletcher AN (1982) Fluorescence quantum yields of some rhodamine dyes. J Lumin 27:455–462. https://doi.org/10.1016/0022-2313(82)90045-X

34. Frisch MJ et al (2009) Gaussian 09, revision A.1. Gaussian, Inc., Wallingford

35. Tomasi J, Mennucci B, Cammi R (2005) Quantum mechanical continuum solvation models. Chem Rev 105:2999–3093. https://doi.org/10.1021/cr9904009

36. Dennington R, Keith T, Millam J (2009) GaussView, Version 5. Semichem, Inc., Shawnee

37. Liu T, Chien AD, Lu J, Zhang G, Fraser CL (2011) Arene effects on difluoroboron β-diketonate mechanochromic luminescence. J Mater Chem 21:8401–8408. https://doi.org/10.1039/c0jm04326e

38. Morris WA, Liu T, Fraser CL (2015) Mechanochromic luminescence of halide-substituted difluoroboron β-diketonate dyes. J Mater Chem C 3:352–363. https://doi.org/10.1039/C4TC02268H

39. Pople JA, Gordon M (1967) Molecular orbital theory of the electronic structure of organic compounds. I Substituent effects and

dipole moments. J Am Chem Soc 89:4253–4261. https://doi.org/10.1021/ja00993a001

40. Werner TC, Lyon DB (1982) Empirical measures of solvent effects on the fluorescence energy of methyl anthroates. J Phys Chem 86:933–939. https://doi.org/10.1021/j100395a019

41. Baragi JG, Aralaguppi MI, Aminabhavi TM, Kariduraganavar MY, Kulkarni SS (2005) Density, viscosity, refractive index, and speed of sound for binary mixtures of 1,4-dioxane with different organic liquids at (298.15, 303.15, and 308.15) K. J Chem Eng Data 50:917–923. https://doi.org/10.1021/je049609w

42. Zhang G, Lu J, Fraser CL (2010) Mechanochromic luminescence quenching: force-enhanced singlet-to-triplet intersystem crossing for iodide-substituted difluoroboron-dibenzoylmethane-dodecane in the solid state. Inorg Chem 49:10747–10749. https://doi.org/10.1021/ic902591s